Linear scheme for time-domain fluorescence molecular tomography

Feng Gao (高 峰), Wei Liu (刘 维), and Huijuan Zhao (赵会娟)

College of Precision Instrument and Optoelectronics Engineering, Tianjin University, Tianjin 300072

Received January 5, 2006

Based on the generalized pulse spectrum technique that was previously developed for time-domain diffuse optical tomography, we propose a linear framework of time-domain fluorescence molecular tomography for simultaneous reconstruction of both the yield and lifetime of multi-fluorophores. The methodology is exemplified for mono-component case and validated with simulated data.

OCIS codes: 170.3880, 170.5280, 170.3010.

With the maturity of near infrared (NIR) fluorescence diffuse optical tomography (DOT)[1] and advances in molecule-specific red-shifted and NIR fluorescent probes[2], fluorescence molecular tomography (FMT) is evolving as a novel optical imaging modality for visualization and quantification of the gene function and expression deep inside intact living subjects[3,4]. FMT has been successfully demonstrated in continuous-wave[5] and frequency-domain modes[6]. Its extension to time-domain (TD) mode is imminent[7,8], where not only the simultaneous recovery of fluorescent yield and lifetime but also the analysis of multiple components could be achieved in a direct way. The two-parameter reconstruction provides information concerning not only the localization but also the local environment (oxygen, $[Ca^{2+}]$, pH value) of fluorophores, while the multi-component analysis enables assessment of multi-gene controlling mechanism in a disease progression. As with the TD-DOT, TD-FMT can also be performed using either the full time-resolved scheme[9] or the featured-data one[10], with the former better quantifying the reconstruction but at the large computation cost as well as high noise-sensitivity, while the latter being fast and robust but with degraded quantification because of the information loss[9]. By extending the generalized pulse spectrum technique (GPST), which is a featured-data scheme previously developed for TD-DOT, we propose a linear TD-FMT algorithm for simultaneously reconstructing both the yield and lifetime distributions of multiple fluorescent components. The methodology is exemplified for one-component case and validated with simulated data.

The image reconstruction in FMT is expressed as an inverse issue for a given photon-migration model, which prevalently employs the photon diffusion equation[10]. In complex domain, the coupled diffusion equations that govern the relationship between the excitation and emission propagations in turbid medium as excited by an ideal ultra-short point source are given as

$$\begin{cases} \left[\nabla\cdot D_{\mathrm{x}}\left(\mathbf{r}\right)\nabla-\mu_{\mathrm{ax}}\left(\mathbf{r}\right)c-p\right]\Phi_{\mathrm{x}}\left(\mathbf{r},p\right) \\ =-\delta\left(\mathbf{r}-\mathbf{r}_{\mathrm{s}}\right) \\ \left[\nabla\cdot D_{\mathrm{m}}\left(\mathbf{r}\right)\nabla-\mu_{\mathrm{am}}\left(\mathbf{r}\right)c-p\right]\Phi_{\mathrm{m}}\left(\mathbf{r},p\right) \\ =-\Phi_{\mathrm{x}}\left(\mathbf{r},p\right)\sum_{n}^{N_c}\eta\mu_{afn}\left(\mathbf{r}\right)/\left[1+p\tau_n\left(\mathbf{r}\right)\right] \end{cases}, \quad (1)$$

where subscripts x and m denote the excitation and emission wavelengths, respectively; $\Phi_{\mathrm{v}}\left(\mathbf{r},p\right)$ $(\mathrm{v}\in[\mathrm{x},\mathrm{m}])$ is the Laplace transform of the TD photon density $\Phi_{\mathrm{v}}\left(\mathbf{r},t\right)$; the optical parameters involved are absorption coefficient $\mu_{\mathrm{av}}\left(\mathbf{r}\right)$, reduced scattering coefficient $\mu'_{\mathrm{sv}}\left(\mathbf{r}\right)$, and diffusion coefficient $D_{\mathrm{v}}\left(\mathbf{r},t\right)=c/[3\mu'_{\mathrm{sv}}\left(\mathbf{r}\right)]$; the fluorescent parameters are yield $\eta\mu_{afn}\left(\mathbf{r}\right)$ and lifetime $\tau_n\left(\mathbf{r}\right)$ with n indexing the N_c fluorophores. We employ uniquely the Robin boundary condition (RBC) for the above coupled equations[10],

$$\Phi_{\mathrm{v}}\left(\mathbf{r},p\right)+\frac{2(1-R_{\mathrm{f}})}{1+R_{\mathrm{f}}}D\left(\mathbf{r}\right)\mathbf{n}\cdot\nabla\Phi_{\mathrm{v}}\left(\mathbf{r},p\right)\Big|_{\mathbf{r}\in\partial\Omega}=0, \quad (2)$$

where $R_{\mathrm{f}}\approx 0.53$ is the internal reflection coefficient at the air-tissue boundary. The measurable flux, i.e., the data-type, at the boundary site ξ_d $(d=1,2,\cdots,D)$ and for the source site ζ_s $(s=1,2,\cdots,S)$, is calculated by Fick's law with exploiting the RBC.

$$\Gamma_{\mathrm{v}}\left(\xi_d,\zeta_s,p\right)=\frac{1+R_{\mathrm{f}}}{2(1-R_{\mathrm{f}})}c\Phi_{\mathrm{v}}\left(\xi_d,\zeta_s,p\right). \quad (3)$$

Equation (1) can be efficiently solved using the Galerkin finite-element-method (FEM) by expanding $\Phi_{\mathrm{v}}\left(\mathbf{r},t\right)$ into finite elements: $\Phi_{\mathrm{v}}\left(\mathbf{r},p\right)\approx\mathbf{\Phi}_{\mathrm{v}}\left(p\right)^{\mathrm{T}}\mathbf{u}\left(\mathbf{r}\right)$ with $\mathbf{u}\left(\mathbf{r}\right)=\left[u_1\left(\mathbf{r}\right),\ u_2\left(\mathbf{r}\right),\ \cdots,\ u_N\left(\mathbf{r}\right)\right]^{\mathrm{T}}$ and $\mathbf{\Phi}_{\mathrm{v}}\left(p\right)=\left[\Phi_{\mathrm{v}}\left(1,p\right),\ \Phi_{\mathrm{v}}\left(2,p\right),\ \cdots,\ \Phi_{\mathrm{v}}\left(N,p\right)\right]^{\mathrm{T}}$ denoting the shape function and Laplace-transformed photon density at the N nodes of the FEM mesh, resulting in the following matrix equation

$$\left(\mathbf{A}_{\mathrm{v}}+\mathbf{B}\right)\mathbf{\Phi}_{\mathrm{v}}\left(p\right)=\mathbf{Q}_{\mathrm{v}}, \quad (4)$$

where $\mathbf{A}_{\mathrm{v}}$ and $\mathbf{B}$ are of the same expression for the excitation and emission[10], but $\mathbf{Q}_{\mathrm{v}}$ differs in form for the excitation and emission as

$$Q_{\mathrm{v}}\left(i,t\right)=\begin{cases} \int_{\Omega}u_i\left(\mathbf{r}\right)\delta\left(\mathbf{r}-\mathbf{r}_{\mathrm{s}}\right)\mathrm{d}\Omega=u_i\left(\mathbf{r}_{\mathrm{s}}\right) \\ \qquad\text{for } \mathrm{v}=\mathrm{x} \\ \sum_{j=1}^{N}C\left(i,j\right)\Phi_{\mathrm{x}}\left(j,p\right)\sum_{n}^{N_c}\frac{\eta\mu_{afn}(j)}{1+p\tau_n(j)} \\ \qquad\text{for } \mathrm{v}=\mathrm{m} \end{cases}, \quad (5)$$

where i and j index the N nodes of the mesh; $\eta\mu_{afn}\left(j\right)$ and $\tau_n\left(j\right)$ the yield and lifetime of the nth fluorophore at the jth meshing node, respectively.

According to Eq. (1) and considering the Fick's Law at

the emission wavelength, we obtain an integral equation as

$$\begin{cases} \Gamma_{\rm m}(\xi_d,\zeta_s,p) \\ \quad = \int_\Omega G_{\rm m}(\xi_d,\mathbf{r},p)\,\Phi_{\rm x}(\mathbf{r},\zeta_s,p)\,x(\mathbf{r},p)\,{\rm d}\Omega \\ x(\mathbf{r},p) = \sum_n^{N_c} \eta\mu_{afi}(\mathbf{r})/[1+p\tau_n(\mathbf{r})] \end{cases}, \quad (6)$$

where $\Gamma_{\rm m}(\xi_d,\zeta_s,p)$ is Laplace transform of the measured TD flux for a source-detector combination and $G_{\rm m}(\mathbf{r},\mathbf{r}',p)$ the Green's function (flux) of the diffusion equation at the emission wavelength. Let $\mathbf{\Gamma}(p) = [\Gamma_{\rm m}(\xi_1,\zeta_1,p),\ \Gamma_{\rm m}(\xi_2,\zeta_1,p),\ \cdots,\ \Gamma_{\rm m}(\xi_D,\zeta_S,p)]^{\rm T}$, and $x(\mathbf{r},p) \approx \mathbf{x}^{\rm T}(p)\mathbf{u}(\mathbf{r})$ with $\mathbf{x}(p) = [x_1(p),\ x_2(p),\ \ldots,\ x_N(p)]^{\rm T}$, Eq. (6) can be discretized into a matrix equation

$$\mathbf{\Gamma}(p) = \mathbf{W}(p)\,\mathbf{x}(p), \quad (7)$$

with the entries of the weighting matrix $\mathbf{W}(p)$ given by

$$W_{ds}(\xi_d,\zeta_s,p,n) = \sum_{\Omega_n} \bar{G}_{\rm m}^{(\Omega_n)}(\xi_d,p)\,\bar{\Phi}_{\rm x}^{(\Omega_n)}(\zeta_s,p)\int_{\Omega_n} u_n(\mathbf{r})\,{\rm d}\Omega, \quad (8)$$

where Ω_n numerates all the elements that are joined at the nth node; $\bar{G}_{\rm m}^{(\Omega_n)}(\xi_d,p)$ and $\bar{\Phi}_{\rm x}^{(\Omega_n)}(\zeta_s,p)$ are the mean values of $G_{\rm m}(\xi_d,\mathbf{r},p)$ and $\Phi_{\rm x}(\mathbf{r},\zeta_s,p)$ over the nodes of the element Ω_n, respectively. For solving Eq. (7) that is usually of large scale and ill-posed, the algebraic reconstruction technique (ART) might be very efficient, where the initial point $\mathbf{x}_0(p)$ is set homogeneous to those for the background. In principle, the ART sequentially projects a solution estimate onto the hyperplanes defined by the individual rows of Eq. (7). The relaxation factor λ, which has a significant influence on the results, has been proven in a range of [0, 2] to make the algorithm converge to a point on the intersection of the governing equations that is nearest to the initial point. The regularization strategy in an ART-based algorithm is accomplished by limiting the number of iterations, whose choice is task-dependent and mandatory in presence of noise. The primary advantage of this implicit linear method over other solutions to a linear system, such as the Levenberg-Marquardt (LM), the truncated singular-value-decomposition (SVD), and conjugate-gradient (CG) algorithms, is its near independence of memory occupation since only one row in the weight matrix is needed at one time.

In principle, the yield and lifetime images of multiple components can be found from $x(\mathbf{r},p)$ using at least $2N_{\rm c}$ working frequency pairs in the Laplace transforms. As an example, the yield $\eta\mu_{af}(\mathbf{r})$ and lifetime $\tau(\mathbf{r})$ in one-component case can be simply recovered from the images of $x(\mathbf{r},p_1)$ and $x(\mathbf{r},p_2)$, for a pair of the real-domain working frequencies, saying p_1 and p_2,

$$\begin{cases} \eta\mu_{af}(\mathbf{r}) = \frac{(p_1-p_2)x(\mathbf{r},p_1)x(\mathbf{r},p_2)}{p_1x(\mathbf{r},p_1)-p_2x(\mathbf{r},p_2)} \\ \tau(\mathbf{r}) = -\frac{x(\mathbf{r},p_1)-x(\mathbf{r},p_2)}{p_1x(\mathbf{r},p_1)-p_2x(\mathbf{r},p_2)} \end{cases}. \quad (9)$$

For computational simplicity, the validation of the methodology is performed on a two-dimensional (2D) circular domain with a diameter of $R = 25$ mm, using simulated data with Gaussian additive noise, i.e.,

$$\Gamma_{\rm m}(\xi_d,\zeta_s,p) = \hat{\Gamma}_{\rm m}(\xi_d,\zeta_s,p)\left(1+10^{-\chi/20}R_N\right), \quad (10)$$

where $\hat{\Gamma}_{\rm m}(\xi_d,\zeta_s,p)$ stands for the calculated (noiseless) data-type from Eq. (1), χ the signal-to-noise ratio (SNR) in decibels, and R_N the standard normal distributed random number. Nevertheless, the principle of the methodology is applicable to three-dimensional (3D) models of the realistic geometry. For applying FEM, the domain is divided into 3750 triangles that join at 1951 nodes. Sixteen optodes with coaxial source-detector structure are assumed around the annulus at equal spacing, of which the 16 detectors collect the exiting photons in parallel while the 16 sources illuminate the surface successively. Of the total 256 TD measurements, only 9 measurements from the detectors opposite to the illuminating source (transmission mode), i.e., a set of 144 TD data, are employed in the reconstruction to effectively reduce the difference in the order of the data magnitude and therefore to significantly improve the image quality[9]. Figure 1 shows the FEM mesh and the source-detector deployment.

To simulate complex situations that are probably encountered in practice, 4 circular fluorescent targets with the unique diameter of $r = 4$ mm but different fluorescent properties are embedded in the 2D domain. The optical properties of the targets in both the cases are the same as those of the background, that are chosen in the range of the optical properties for *in vivo* muscle, i.e., $\mu_{\rm ax,m} = 0.035$ mm^{-1} and $\mu'_{\rm sx,m} = 1.0$ mm^{-1} at both the excitation and emission wavelengths. Table 1 lists the geometric parameters, optical and fluorescent properties of the phantom.

Firstly, the image reconstruction is performed for a variety of SNRs, with a fixed working frequency pair of $p_{1,2} = \mp 0.25P$, where $P = 1/\left[1/\mu_{\rm ax}^{(B)}c + 1/\mu_{\rm am}^{(B)}c + \tau^{(B)}\right]$, aiming at evaluating the ability of the algorithm to distinguish the difference in both fluorescent yield and lifetime of the targets and its

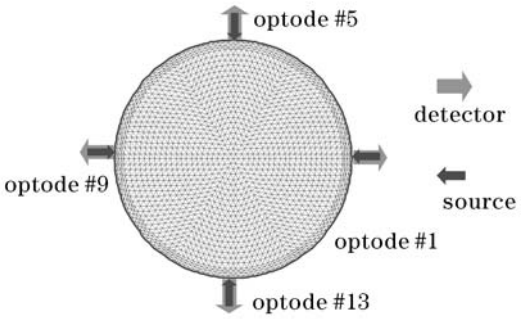

Fig. 1. FEM mesh and optode deployment employed in the study.

Table 1. Optical, Fluorescent and Geometrical Parameters of Case 1

Region	Diameter (mm)	$\mu_{\rm ax,m}$ (mm^{-1})	$\mu'_{\rm sx,m}$ (mm^{-1})	$\eta\mu_{af}$ (mm^{-1})	τ (ps)
Background	25	0.035	1.0	0.001	100
Target 1	4	0.035	1.0	0.0015	500
Target 2	4	0.035	1.0	0.0025	300
Target 3	4	0.035	1.0	0.003	400
Target 4	4	0.035	1.0	0.002	600

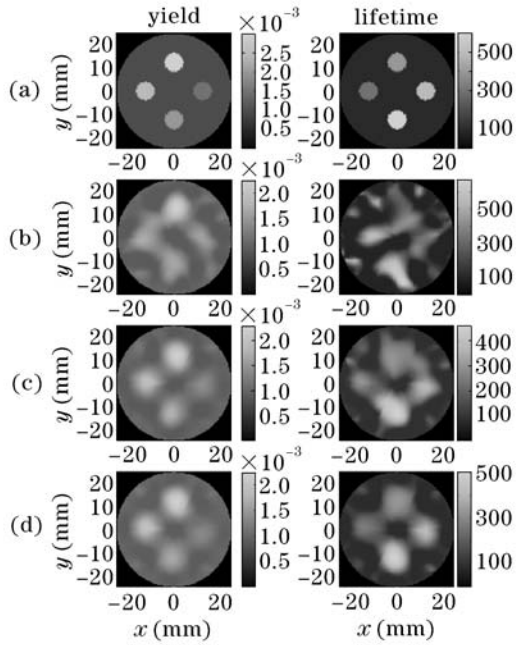

Fig. 2. Reconstructed fluorescent yield and lifetime images of the numerical phantom with noisy data at different SNRs of 30 (b), 40 (c), and 50 dB (d) for a working frequency pair $\mp 0.25P$, together with the original images (a) for comparison.

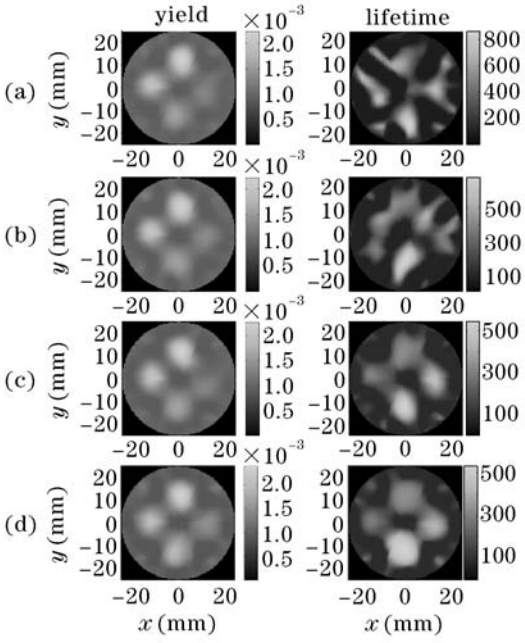

Fig. 3. Reconstruction of the numerical phantom using noisy data at a fixed SNR of 40 dB for different working frequency pairs: $\mp 0.05P$ (a), $\mp 0.1P$ (b), $\mp 0.25P$ (c), and $\mp 0.5P$ (d).

noise-robustness. Figure 2 shows the original and reconstructed images at different SNRs of 30, 40, and 50 dB, where all the differences among the targets in both the yield and lifetime are fairly disclosed at a moderate SNR higher than 40 dB. Further improvements in spatial resolution and quantitative accuracy are desired in future work. Secondly, we investigate the influence of choice of working frequencies on the image quality by reconstructing the images using a variety of working frequency pairs: $p_{1,2} = \mp 0.05P$, $\mp 0.1P$, $\mp 0.25P$, $\mp 0.5P$, and $\mp 0.75P$, respectively, at a fixed SNR of 40 dB, as shown in Fig. 3. It is observed that, with the difference between the paired frequencies enlarged, the image quality, especially for the lifetime image, is significantly improved. An optimal image quality can be attained approximately at $p_{1,2} = \mp 0.5P$, after which the image quality again increasingly degrades (the images not shown here). It is therefore concluded that to obtain a maximum fidelity of reconstruction in presence of noise, an optimized frequency pair might be practically crucial to the detection of the faint fluorescent light.

In summary, we have presented a linear GPST methodology of TD-FMT for simultaneous reconstruction of the fluorescent yield and lifetime of multiple components, from which the algorithm for one-component recovery was exemplified. The simulative validations of the algorithm for a 2D domain have been performed for its capability of discerning the difference in the fluorescent properties and noise-robustness. The resultant images have fairly demonstrated the effectiveness of the proposed methodology. In addition, we have investigated the influence of the paired working frequencies on the reconstruction and concluded that an optimal choice of the working frequency pair can greatly enhance the noise-robustness of the algorithm. In the on-going work, the phantom and *in vivo* experimental validations of the methodology will be explored.

This work was supported by the National Natural Science Foundation of China (No. 60578008) and National Basic Research Program of China (No. 2006CB705700). F. Gao's e-mail address is gaofeng@tju.edu.cn.

References

1. E. M. Sevick-Muraca, J. P. Houston, and M. Gurfinkel, Current Opinion in Chemical Biology **6,** 642 (2002).
2. K. Licha, Topics in Current Chemistry **222,** 1 (2002).
3. T. F. Massoud and S. S. Gambhir, Genes and Development **17,** 5450 (2003).
4. S. R. Cherry, Phys. Med. Biol. **49,** R13 (2004).
5. V. Ntziachristos, C. H. Tung, C. Bremer, and R. Weissleder, Nature Medicine **8,** 757 (2002).
6. X. Cong and G. Wang, Opt. Express **13,** 9847 (2005).
7. S. Lam, F. Lesage, and X. Intes, Opt. Express **13,** 2263 (2005).
8. A. T. N. Kumar, J. Skoch, B. J. Bacskai, D. A. Boas, and A. K. Dunn, Opt. Lett. **30,** 3347 (2005).
9. F. Gao, H. Zhao, and Y. Yamada, Appl. Opt. **41,** 778 (2002).
10. S. R. Arridge, Inverse Problems **15,** R41 (1999).